LAWRENCE
LIVERMORE
NATIONAL
LABORATORY

UCRL-CONF-236317

Energetics of Multiple-Ion Species Hohlraum Plasmas

P. Neumayer, R. Berger, D. Callahan, L. Divol, D. Froula, R. London, B. J. MacGowan, N. Meezan, P. Michel, J. S. Ross, C. Sorce, K. Widmann, L. Suter, S. H. Glenzer

November 7, 2007

American Physical Society
Orlando, FL, United States
November 12, 2007 through November 16, 2007

Disclaimer

Energetics of Multiple-Ion Species Hohlraum Plasmas

P. Neumayer,* R. L. Berger, D. Callahan, L. Divol, D. H. Froula,
R. A. London, B. J. MacGowan, N. B. Meezan, P. A. Michel, J.
S. Ross, C. Sorce, K. Widmann, L. J. Suter, and S. H. Glenzer
L-399, Lawrence Livermore National Laboratory,
University of California, P.O. Box 808, Livermore, CA 94551, USA

(Dated: November 5, 2007)

Abstract

A study of the laser-plasma interaction processes in multiple-ion species plasmas has been performed in plasmas that are created to emulate the plasma conditions in indirect drive inertial confinement fusion targets. Gas-filled hohlraums with with densities of xe22/cc are heated to Te=3keV and backscattered laser light is measured by a suite of absolutely calibrated backscatter diagnostics. Ion Landau damping is increased by adding hydrogen to the CO2/CF4 gas fill. We find that the backscatter from stimulated Brillouin scattering is reduced is monotonically reduced with increasing damping, demonstrating that Landau damping is the controlling damping mechanism in ICF relevant high-electron temperature plasmas. The reduction in backscatter is accompanied by a comparable increase in both transmission of a probe beam and an increased hohlraum radiation temperature, showing that multiple-ion species plasmas improve the overall hohlraum energetics/performance. Comparison of the experimental data to linear gain calculations as well as detailed full-scale 3D laser-plasma interaction simulations show quantitative agreement. Our findings confirm the importance of Landau damping in controlling backscatter from high-electron temperature hohlraum plasmas and have lead to the inclusion of multi-ion species plasmas in the hohlraum point design for upcoming ignition campaigns at the National Ignition Facility.

PACS numbers: 52.25.Os, 52.35.Fp, 52.50.Jm

*Electronic address: neumayer2@llnl.gov

I. INTRODUCTION

In the indirect-drive approach to Inertial Confinement Fusion [?] (ICF) a deuterium-tritium filled fusion capsule is compressed by the ablation pressure from soft x-rays inside a laser heated radiation cavity (hohlraum). With the National Ignition Facility (NIF) [?] nearing completion, 192 laser beams with a total UV energy of $> 1\,\mathrm{MJ}$ will be available to heat cm-scale hohlraums to radiation temperatures of 270-300 eV. To reach these required radiation temperatures, the laser beams have to efficiently propagate over a length of 3-7 millimeter through underdense plasma at electron temperatures of $T_e = 2.5 - 5\,\mathrm{keV}$ before depositing their energy into the hohlraum wall [?]. Stimulated scattering processes in both the high-Z blow-off plasma from the hohlraum wall and the low-Z gas-fill plasma can backscatter the laser light by parametric laser-plasma instabilities, i.e. Stimulated Brillouin Scattering (SBS) and Stimulated Raman Scattering (SRS). These processes strongly depend on laser and plasma conditions; the latter need to be taylored to optimize soft x-ray drive and radiation symmetry required to compress the fusion fuel to ignition conditions.

Recent studies have focused on the importance of reducing peak laser beam speckle intensities by employing Continuous Phase Plates (CPP) [? ?] and advanced beam smoothing techniques such as Polarization Smoothing (PS) and Smoothing by Spectral Dispersion (SSD) [? ? ? ?]. These techniques have been shown to result in improved coupling into gas filled hohlraums [? ?] and cryogenic gas bag targets [?].

An important plasma parameter in controlling laser-plasma interactions is plasma wave damping. At the high electron temperature laser heated plasma conditions, typical in ICF targets, ion Landau damping in single-ion species plasmas is negligible. Landau damping due to electrons is small and of the order of 0.01, due to the large mass difference between electrons and ions. However, in multiple ion species plasmas, the number of charged particles close to the phase velocity of the SBS driven fast ion-acoustic mode is greatly enhanced effectively providing Landau damping.

A long-standing problem in the field of laser-plasma interactions is a successful demonstration that multiple-ion species plasmas lead to reduced backscattering at ICF hohlraum conditions. Although the effect of two-ion species plasmas on Landau damping has been directly observed with Thomson scattering [? ?], previous laser-plasma interaction experiments have not observed the expected reduction of SBS reflectivity with increased Landau

damping. In addition, the experiments showed that SRS strongly increased reaching levels of more than 20% [? ? ?]. These experiments have been performed with a limited set of beam smoothing options or in low temperature plasmas where laser beam filamentation exceeds the growth threshold.

In this letter, we demonstrate for the first time that laser backscattering processes are strongly suppressed in multiple-ion species plasmas that approach ignition conditions. Adding hydrogen to a hohlraum filled with CO_2 is shown to reduce SBS reflected energy from 20% to the percent level. This is accompanied by a simultaneous increase of the transmitted energy of an axial interaction laser beam and increased radiation temperature of the hohlraum. These experiments were performed in high electron temperature hohlraums that have been heated employing beam smoothing (CPP and PS), thus avoiding laser beam filamentation. The measured scaling of SBS with increasing Landau damping agrees with linear gain calculations. Full scale 3D laser-plasma interaction simulations reproduce these findings and further indicate that SBS can be efficiently controlled by employing multiple-ion species plasmas on future ICF experiments on the NIF.

II. EXPERIMENT

A. High Electron-Temperature Targets

Figure 1 shows a schematic of the experimental configuration. The experiments were performed at the Omega laser facility at the Laboratory for Laser Energetics (LLE), Rochester [?]. Cylindrically shaped gold hohlraums (2 mm length, 1.6 mm diameter) were filled with ≈1 atm of CO_2. The fill pressure was chosen to yield an electron density of $0.06 \cdot n_{\text{crit.}}$ where $n_{\text{crit.}} \approx 10^{22}\text{cm}^{-3}$ is the critical density up to which light of wavelength $\lambda = 351\,\text{nm}$ can propagate. Hydrogen was added to this gas fill as a light ion species by adding a small amount of up to 13 % of propane (C_3H_8) and adjusting the total fill pressure to maintain the electron density constant.

The hohlraum targets were heated by 33 (351 nm) heater beams to radiation temperatures of 235 eV as measured by the absolutely calibrated soft x-ray DANTE detector. The heater beams enter the hohlraum through 2 laser entrance holes (LEH) of 800 μm diameter on either side of the hohlraum. The LEH are covered with 0.25 μm thick polyimide windows to

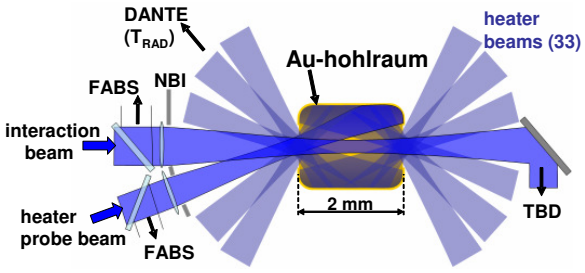

FIG. 1: Schematic of the experimental setup. The cylindrical hohlraum is heated by 33 heater beams with 14.3 kJ of energy in a 1 ns long square pulse. The backscattered light from one of the heater beams and an on-axis probe beam is measured by FABS and NBI (see text) and the transmitted laser energy by TBD. The hohlraum radiation temperature is measured by DANTE.

hold the gas fill. The beams are arranged in 3 cones with entrance angles of 20, 42 and 60 degrees to the hohlraum axis. In this study we have employed phase plates and polarization smoothing on all heater beams. The $200 \times 300\,\mu$m elliptical focal spots have been oriented such that the projection onto the LEH was close to circular. Polarization smoothing using Distributed Phase Rotators was employed to reduce peak intensities from speckles in the focal intensity distribution.

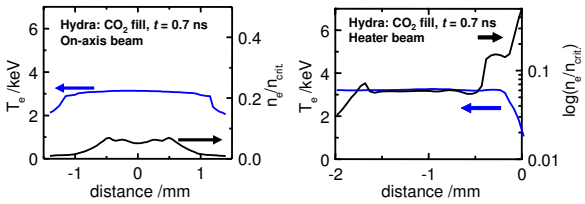

FIG. 2: Electron density and temperature profiles along the on-axis and the heater interaction probe beam, as obtained from radiation hydrodynamic calculations using HYDRA. The electron temperatures of 3 keV agree with Thomson scattering measurements.

Typical laser energies of 435 J per heater beam result in an intensity of $9 \times 10^{14}\,\mathrm{W/cm^2}$ at the hohlraum wall, well below the threshold intensity for filamentation ([? ?]) $I_{\mathrm{thresh.}} \propto T_\mathrm{e}/n_\mathrm{e} \approx 1.7 \times 10^{15}\,\mathrm{W/cm^2}$ for our conditions. The hohlraum target platform has been extensively studied in earlier experiments (see e.g. [?]). Using Thomson scattering the electron temperature has been measured to reach peak values of 3.5 keV. This is in good agreement with 2-D radiation-hydrodynamic simulations using the code HYDRA [?], see fig. 2. These show a homogenous electron density distribution along the center axis of the

hohlraum. For the heater beam the electron density rapidly however rises rapidly towards the hohlraum wall.

In addition to the heater beams, an axial laser-plasma interaction probe beam of 351 nm wavelength was propagated along the cylinder axis. A continuous phase plate was used to achieve a focal spot size of 250 μm at the center of the hohlraum. The probe beam was delayed by 0.3 ns with respect to the heater beams. The intensity of the probe beam was varied between 3.6×10^{14} and 1.2×10^{15} W/cm^2 by varying the total energy of the 1 ns long square pulse between 140–480 J.

The backscattered light from the axial probe beam and from one of the heater beams is measured by the Full Aperture Backscatter Station (FABS) and the Near Backscatter Imager (NBI) while the Transmitted Beam Diagnostic (TBD) measures the transmitted laser light of the on-axis probe beam. The FABS measures the light backscattered into the final focusing lens aperture by down-collimating the reflection off the front surface of a full-aperture uncoated glass wedge in the beamline onto a diagnostics table. Time-resolved spectra are recorded by two streaked spectrometers covering the wavelength range of (351 ± 3)nm for SBS and 450-700 nm for SRS. The total backscattered energy in either of those spectral ranges is measured by calorimeters. The energy response had been calibrated by propagating a known beam energy from the target chamber center directly into the instrument. We estimate the absolute uncertainty in the energy measured by the FABS to $\pm 5\%$.

Near-backscattered light outside the FABS aperture is measured by the NBI. This light is diffusely scattered from spectralon coated Aluminum plates surrounding the lens apertures and is imaged onto two CCD cameras, spectrally filtered for the SBS and SRS wavelength range. The response of the NBI is calibrated in both wavelength regimes by locally illuminating the scatter plate with individual laser pulses of known energy (mJ) at wavelengths of 355 nm and 532 nm. The total backscattered energy on the NBI plate is determined from the CCD image with an uncertainty of $\pm 10\%$. In these experiments the energy measured with the NBI was small and of the order of a few percent of the energy measured in FABS, consistent with filamentation being negligible in these experiments.

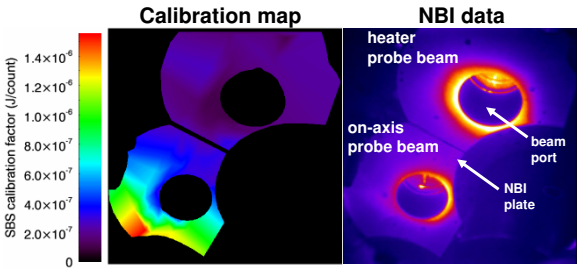

FIG. 3: Calibration map optained from the NBI pulsed calibration system (left) and typical NBI data (right). In the image shown the energy on the NBI was 28 J (i.e. 0.25× the energy measured by FABS) for the heater probe beam and 15 J (i.e. 0.15× FABS) for the on-axis probe beam.

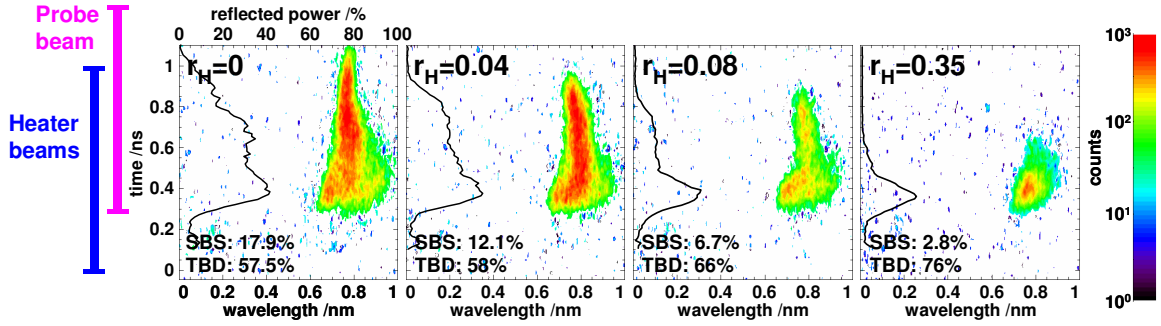

FIG. 4: Streaked spectra of the backscattered light from the axial interaction probe beam. The hydrogen fraction r_{H} and the backscattered and transmitted energies are denoted in the images. The probe beam intensity in these shots was $I = 3.6 \times 10^{14}\mathrm{W/cm^2}$. The images are corrected for differences in neutral-density filtering from shot to shot. The lineouts shows the fraction of scattered SBS power.

III. RESULTS AND DISCUSSION

A. On-axis interaction probe beam results

Figure 4 shows time-resolved spectra from the FABS SBS channel backscattered from the probe beam at an intensity of $3.6 \times 10^{14}\,\mathrm{W/cm^2}$. The hydrogen fraction in these shots increases from $r_{\mathrm{H}} = 0$, 0.04, 0.08 to 0.35. The data clearly shows the backscatter from SBS being reduced with increasing hydrogen fraction. The total backscattered energy as measured by the FABS was reduced by more than a factor of 6 from 18% to 2.6%. Simultaneously, the total transmitted energy of the probe beam increases by approximatly the same amount such that the sum of SBS backscattered and transmitted beam energy

remains roughly constant in the range of 70-80 %. The spectra show a spectrally narrow feature red-shifted by ≈ 0.8 nm from the incident laser wavelength, indicating that SBS is driven in the bulk of the plasma at temperatures of $\approx 3\,\mathrm{keV}$. The reflectivity ceases at $t \approx 1\,\mathrm{ns}$ although the probe pulse extends up to $t = 1.3\,\mathrm{ns}$, due to a rapid rise of the ion temperature on-axis when plasma from the hohlraum wall blow-off coalesces on-axis [?].

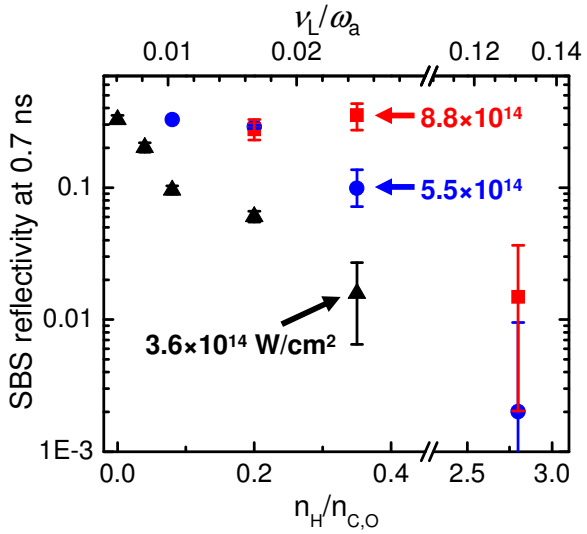

FIG. 5: Instantaneous SBS reflectivities at $t = 0.7\,\mathrm{ns}$ for interaction beam intensities of 3.6, 5.5 and $8.8 \times 10^{14}\,\mathrm{W/cm^2}$. Also shown are the Landau damping values increasing from 0.006 to 0.13.

Also shown in Fig. 4 is the time history of the SBS reflected power showing that adding hydrogen to the gas fill the reflected power is reduced throughout the entire duration of the pulse. However, while at later times ($> 0.5\,\mathrm{ns}$) the effect of the increased Landau damping is strong, at early times (0.3-0.5 ns) the reflectivity is less affected. At this early time the electron temperature is below 2 keV and the SBS instability is strongly driven.

Figure 5 shows the instantaneous SBS reflectivity for varying r_H at $t = 0.7\,\mathrm{ns}$. At this time the plasma electron temperature has increased to $T_\mathrm{e} = 3\,\mathrm{keV}$ [?] so the plasma is in the high electron temperature regime where Landau damping is important in controlling SBS. The ion temperature is $T_\mathrm{i} \approx 400\,\mathrm{eV}$. For the probe beam intensity of $3.6 \times 10^{14}\,\mathrm{W/cm^2}$ the reflected power is gradually reduced from 30 % to the percent level when increasing the hydrogen fraction to $r_\mathrm{H} = 0.35$, i.e. when increasing Landau damping from $\nu_\mathrm{L}/\omega_\mathrm{a} = 0.006$ to $\nu_\mathrm{L}/\omega_\mathrm{a} = 0.025$. For higher probe beam intensities the reflectivity is reduced if higher hydrogen fractions are employed, indicating strong saturation of the SBS instability, e.g., by pump depletion. The error bars are mainly due to the uncertainty in the relative timing of

about 100 ps. We note that in all cases the level of SRS backscattered light was below the instrumental detection threshold, i.e. below $\approx 10^{-4}$.

The reduction of SBS reflectivity with increasing Landau damping is well reproduced by linear gain calculations using plasma parameters obtained from radiation hydrodynamic simulations. For the experimental conditions (laser light distribution inside the hohlraum and gas fill), electron and ion temperatures, densities and flow velocities are obtained from HYDRA calculations and subsequently post-processed with the Laser Interaction Post-Processor LIP [? ?] to calculate temporally and spectrally resolved linear gains for SBS along the path of the probe beam. Fig. 6 shows a comparison of streaked spectra with the results from LIP gain calculations. The good agreement demonstrates the accuracy of 2D hydro simulations.

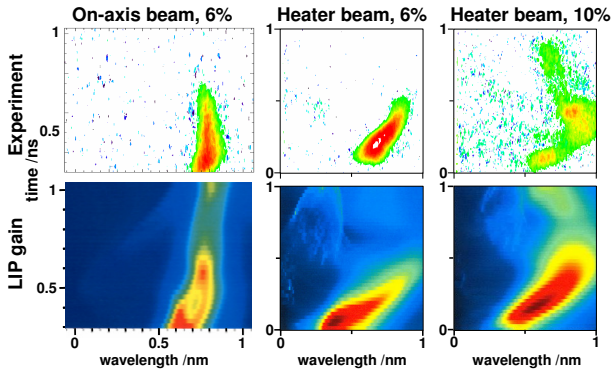

FIG. 6: Comparison of measured streaked spectra with linear gain calculations (LIP). The spectral-temporal evolution reflects the hydrodynamic evolution of the hohlraum plasma.

Figure 7 shows the scaling of the SBS reflectivity at $t = 0.7\,\mathrm{ns}$ as a function of the calculated LIP gain values. These data demonstrate that the backscattered intensity grows exponentially with gain at high-temperature hohlraum conditions. A more quantitative prediction of SBS has been obtained from the 3D laser-plasma interaction code pF3D [?]. These integrated calculations use realistic beams including micrometre-scale speckles. This is important as speckles play a crucial role in triggering SBS thus lowering the experimental threshold for the onset of SBS. Also pump depletion and ponderomotive effects are included. The simulated reflectivities are well within the errors of our measurement and reproduce the effect of SBS being reduced by increased Landau damping while maintaining low SRS reflectivities.

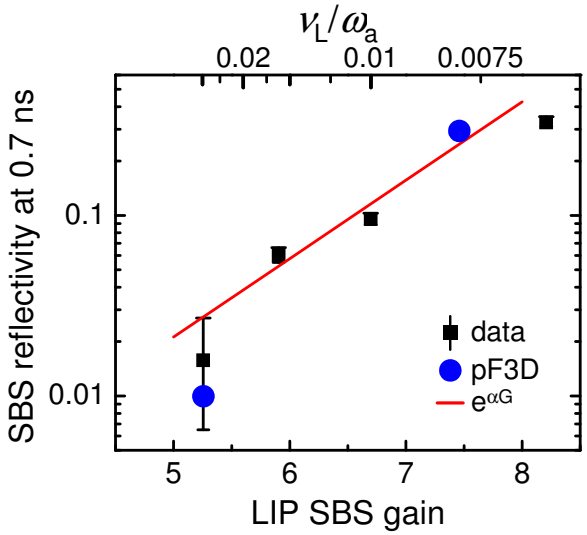

FIG. 7: Scaling of SBS reflectivity (@0.7ns) with LIP gains ($I = 3.6 \times 10^{14}\,\mathrm{W/cm^2}$) shows an exponential growth of backscattered light with the linear gain. Full scale LPI calculations using the code pF3D agree with the observed reflectivities and confirm the trend of reduced backscatter due to increased damping.

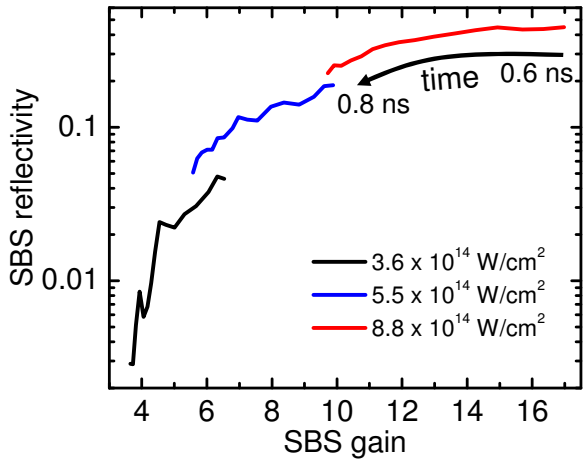

FIG. 8: Instantaneous reflectivity for $t = 0.6 - -0.8$ns for different probe beam intensities (3.6, 5.5, $8.8\times10^{14}\,\mathrm{W/cm^2}$ at $r_H = 0.35$. The reflectivity decrease in time matches with the gain dropping due to increasing Landau damping as the ion temperature rises.

B. Heater probe beam results

Besides the on-axis interaction beam, one of the heater beams was equipped with a full backscatter diagnostics (FABS and NBI). This beam enters the LEH at 20 degrees to the

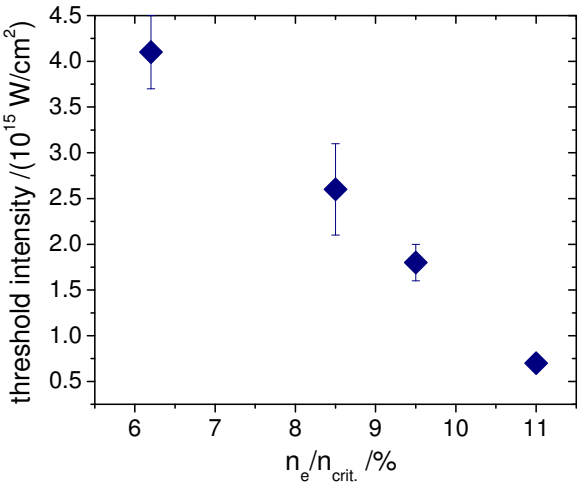

FIG. 9: Intensity threshold for the onset of SRS for ne varying from 6 to 11 %.

cylinder axis and propagates through the hohlraum center until it reaches the hohlraum wall. The heater beam intensity inside the hohlraum is $\approx 9 \times 10^{14}\,\mathrm{W/cm^2}$. As it propagates through the hohlraum it encounters mostly the same plasma conditions as the on-axis probe beam, however, towards the hohlraum wall the density rapidly increases. Consequently SRS gains are higher than for the on-axis interaction beam and the backscattered light has a non-negligible SRS component. SBS and SRS backscattered energies are shown in Fig. 10 for increasing r_{H}, and for two different electron densities ($n_{\mathrm{e}}/n_{\mathrm{crit.}} = 0.06$ and 0.1, respectively). We find the same quantitative dependence on Landau damping as for the on-axis probe beam. With increasing hydrogen fraction the SBS backscatter drops from almost 30% to 8%. The SRS backreflected energy is $< 2\%$ while SBS is strong and increases slightly to 4-7% as SBS is suppressed to below 10%. This might be explained by a certain amount of intensity competion between the two instabilities. As the SRS occurs in the higher densities towards the hohlraum wall strong SBS backscatter in the hohlraum reduces the beam intensity towards the hohlraum wall and lowers the SRS gain. As the SBS is suppressed by the increasing Landau damping when adding hydrogen, the intensity remains high until close to the wall and SRS can grow.

This interpretation is supported by measurements of heater beam filamentation and deflection with the NBI. For gas fills with no hydrogen content (i.e. high SBS backscatter from the gas) the backscatter is symmetric around the beam port. When SBS is supressed by increased Landau damping the backscattered beam is deflected, indicating non-linear

processes of the light at the high electron densities closer to the hohlraum wall. Note that in these cases the energy scattered onto the NBI plates amounted up to $\approx 2/3$ of the total backscattered energy, i.e. 2x the energy measured by the FABS.

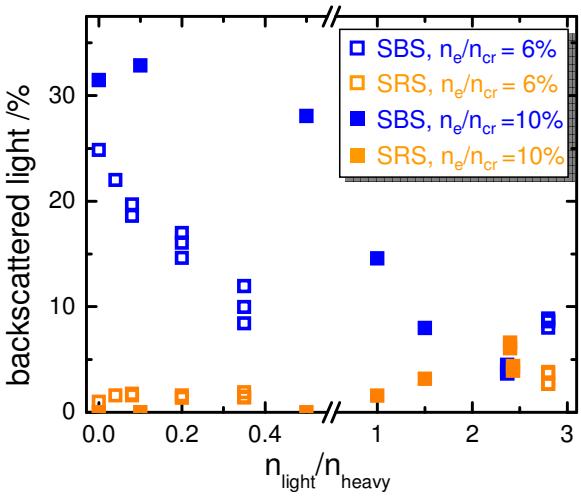

FIG. 10: Time integrated SBS and SRS reflectivity of the heater probe beam (intensity 9e14 W/cm2). While SBS drops form ¿30% to 10% SRS only grows slightly staying below 10%. For the larger electron density (ne/ncrit.=10%) larger damping is required to affect the reflectivities.

High heater beam transmission is essential for efficient deposition of the heater beam energy into the hohlraum wall. As the heater beam backscatter is reduced the intensity in the gold blow-off from the hohlraum wall reaches high levels such that SBS from the slow mode in the gold plasma can grow. Fig. 11 shows streaked SBS spectra from the heater beam. The hydrogen fraction was $r_{\mathrm{H}} = 2.8$ so SBS from the gas was strongly damped. As the SBS from the gas fill ceases after 0.5 ns (i.e. when the electron temperature approaches 3 keV) a narrow feature, shifted by 0.2 nm is observed. This can be attributed to SBS from the slow acoustic mode from the gold plasma. At NIF the outer beams can reach high levels of SBS from this gold plasma. Efficient control of the source of SBS is therefore important. This will be achieved by employing multiple-ion species plasmas. Full-scale laser-plasma interaction calculations using the code pF3D [**?**] have shown that SBS on the outer beams from gold can be suppressed to negligible levels when the hohlraum wall is lined with a gold-boron layer. In our experiments we confirm the effect of adding boron to the gold hohlraum wall. Hohlraum targets with a 150 nm thick layer that contained 20% boron with the gold were shot to compare heater beam backscatter with that from pure gold

hohlraums. As shown in fig. 11 the feature from SBS in gold is efficiently suppressed in the AuB-lined hohlraum. Again, this demonstrates the effectiveness of controlling SBS by increasing Landau damping using multiple-ion species plasmas.

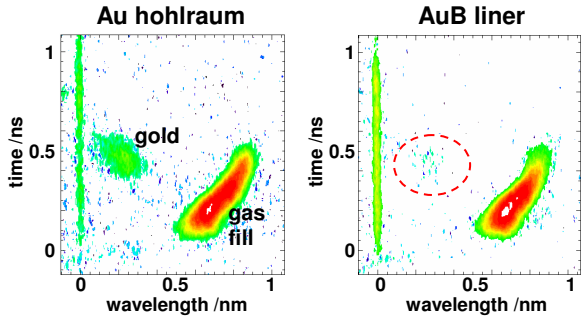

FIG. 11: Fig. x: Streaked SBS spectrum from the backscattered light of the heater beam hitting the hohlraum wall. The strongly shifted feature from the Carbon-like acoustic mode is strongly damped as the electron temperature rises to 3 keV (0.5 ns). At this time the intensity at the hohlraum increases and SBS from the Au hohlraum wall blow-off plasma is observed. A 150 nm thick liner with 20% at of B efficiently suppresses this Au-feature.

C. Hohlraum energetics

The results from the backscatter measurement of the heater beam have shown a strong reduction of the total backscattered energy. This is due to the efficient suppression of SBS that strongly outweighs the slight increase in SRS. The increased amount of laser energy deposited into the hohlraum wall has a measurable effect on the hohlraum energetics. As the hydrogen fraction was raised the hohlraum radiation temperature was measured to increase from 231 eV to 236 eV in a $n_e/n_{crit.} = 0.06$ gas fill and from 226 to 232 eV ($n_e/n_{crit.} = 0.1$). The

Backscatter from heater beams of the outer cones was accounted for based on results from previous experiments [**?**]. The total backscattered heater energy is estimated to be reduced by 8 % (i.e. from 12% to 4%) when increasing r_H. Using a scaling of the peak radiation temperature T_{RAD} based on a flux balance model [**?**] the observed $\Delta T_{RAD} = 4\,eV$ corresponds to an increase in heater energy of 7 % which is in good agreement with the observed change in backscatter.

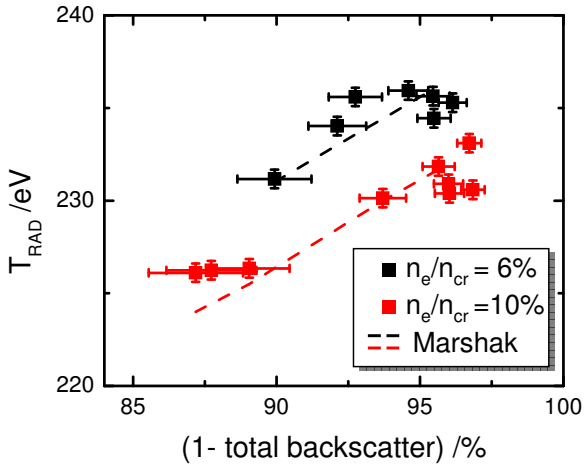

FIG. 12: Fig. x: The increase in peak radiation temperature is correlated to the decrease in backscatter from the heater beams. Predictions from a flux balance model (see text) using the measured amount of backscatter agree quantitatively with the observed ΔT_{RAD}.

IV. SUMMARY AND OUTLOOK

In summary, we have shown that the increasing ion Landau damping in multi-species plasmas strongly suppresses SBS in a high-electron temperature hohlraum plasma. By adding a low-mass ion species (hydrogen) to a CO_2 hohlraum gas fill, the SBS reflected power was reduced from $> 30\%$ to below 1%. The reduction in the total backscattered energy leads to an increased transmission. The suppression of laser backscatter results in an increase of the hohlraum radiation temperature indicating improved coupling of the heater beams. These observations have affected the choice of hohlraum materials and motivated the use of multiple-ion species plasmas for future indirect drive ignition experiments on the NIF. Laser-plasma interaction simulations using pF3D have shown that backscatter from SBS will be suppressed using multiple-ion species plasmas in the hohlraum gas fill and wall blow-off plasma.

V. ACKNOWLEDGMENTS

We would like to acknowledge the efforts of the Omega Laser Crew. These experiments were made possible by D. Hargrove, V. Rekow, J. Armstrong, K. Piston, R. Knight, S. Alverez, R. Griffith, and C. Sorce with their contributions to the 3ωTBD. We thank R.

Wallace and his fabrication team for the robust gas-filled targets. This work performed under the auspices of the U.S. Department of Energy by Lawrence Livermore National Laboratory under Contract DE-AC52-07NA27344.

---

[1] J. D. Lindl, Phys. Plasmas **2**, 3968 (1995).

[2] B. Remington, R. P. Drake, and D. Ryutov, Rev. Mod. Phys. **78**, 755 (2006).

[3] E. Moses *et al.*, Fussion Sci. Tech. **47**, 314 (2005).

[4] C. Cavailler, Plasma Phys. Control. Fusion **47**, B389 (2005).

[5] R. L. Berger, C. Still, E. A. Williams, and A. B. Langdon, Phys. Plasmas **5**, 4337 (1998).

[6] C. Still, R. L. Berger, A. B. Langdon, D. E. Hinkel, L. J. Suter, and E. A. Williams, Phys. Plasmas **7**, 2023 (2000).

[7] W. L. Kruer, *The Physics of laser plasma interactions* (Addison-Wesley Publishing Company, Inc., 1988).

[8] J. D. Lindl, P. A. Amendt, R. L. Berger, S. G. Glendinning, S. H. Glenzer, S. W. Haan, R. L. Kauffman, O. L. Landen, and L. J. Suter, Phys. Plasmas **11**, 339 (2004).

[9] E. A. Williams, Tech. Rep. UCRL-LR-105820-98, Lawrence Livermore National Laboratory (1998).

[10] J. M. Soures, R. L. Mccrory, T. R. Boehly, R. S. Craxton, S. D. Jacobs, J. H. Kelly, T. J. Kessler, J. P. Knauer, R. L. Kremens, S. A. Kumpan, *et al.*, Laser Particle Beams **11**, 317 (1993).

[11] D. Froula, J. Ross, L. Divol, N. Meezan, A. Mackinnon, R. Wallace, and S. Glenzer, Phys. Plasmas **13**, (2006).

[12] S. W. Haan, Phys. Plasmas **2**, 2480 (1995).

[13] S. H. Glenzer, W. Rozmus, B. J. Macgowan, K. G. Estabrook, J. S. De Groot, and G. B. Zimmerman, Phys. Rev. Lett. **82**, 97 (1999).

[14] J. Ross, D. H. Froula, A. J. Mackinnon, C. Sorce, N. Meezan, S. H. Glenzer, W. Armstrong, R. Bahr, R. Huff, and K. Thorp, Rev. Sci. Instrum. **77**, 10E520 (2006).

[15] A. J. Mackinnon, S. Shiromizu, G. Antonini, J. Auerbach, H. Haney, D. H. Froula, J. Moody, G. Gregori, C. Constantin, C. Sorce, et al., Rev. Sci. Instrum. **75**, 3906 (2004).

[16] S. H. Glenzer, T. L. Weiland, J. Bower, A. J. Mackinnon, and B. MacGowan, Rev. Sci.

Instrum. **70**, 1089 (1999).

[17] D. H. Froula, V. Rekow, C. Sorce, K. Piston, R. Knight, S. Alvarez, R. Griffith, D. Hargrove, J. S. Ross, S. Dixit, *et al.*, Rev. Sci. Instrum. **77**, 10E507 (2006).

[18] J. Moody, B. Macgowan, S. Glenzer, R. Kirkwood, W. Kruer, S. Pollaine, E. Williams, G. Stone, B. Afeyan, and A. Schmitt, Rev. Sci. Instrum. **70**, 677 (1999).

[19] J. Moody, B. Macgowan, R. L. Berger, K. G. Estabrook, S. H. Glenzer, R. K. Kirkwood, W. L. Kruer, G. F. Stone, and D. Montgomery, Phys. Plasmas **7**, 3388 (2000).

[20] S. Dixit, M. Feit, M. Perry, and H. Powell, OPT LETT **21**, 1715 (1996).

[21] M. M. Marinak, G. D. Kerbel, N. A. Gentile, O. S. Jones, D. H. Munro, S. Pollaine, T. R. Dittrich, and S. W. Haan, Phys. Plasmas **8**, 2275 (2001).

[22] S. H. Glenzer, W. E. Alley, K. G. Estabrook, J. S. De Groot, M. G. Haines, J. H. Hammer, J. P. Jadaud, B. J. MacGowan, J. D. Moody, W. Rozmus, *et al.*, Phys. Plasmas **6**, 2117 (1999).

[23] G. P. Schurtz, P. Nicolai, and M. Busquet, Phys. Plasmas **7**, 4238 (2000).

[24] B. Macgowan, B. B. Afeyan, C. A. Back, R. L. Berger, G. Bonanno, M. Casanova, B. I. Cohen, D. E. Desenne, D. F. Dubois, A. G. Dulieu, *et al.*, Phys. Plasmas **3**, 2029 (1996).

[25] J. C. Fernandez, B. S. Bauer, K. S. Bradley, J. A. Cobble, D. S. Montgomery, R. G. Watt, B. Bezzerides, K. G. Estabrook, R. Focia, S. R. Goldman, *et al.*, Phys. Rev. Lett. **81**, 2252 (1998).

[26] B. H. Failor, J. Fernandez, B. H. Wilde, A. L. Osterheld, J. A. Cobble, and P. L. Gobby, Physical Review E **59**, 6053 (1999).

[27] R. L. Kauffman, L. V. Powers, S. N. Dixit, S. G. Glendinning, S. H. Glenzer, R. K. Kirkwood, O. L. Landen, B. J. Macgowan, J. D. Moody, T. J. Orzechowski, *et al.*, Phys. Plasmas **5**, 1927 (1998).

[28] D. H. Froula, J. S. Ross, L. Divol, and S. H. Glenzer, Rev. Sci. Instrum. **77**, 10E522 (2006).

[29] J. Sheffield, *Plasma Scattering of Electromagnetic Radiation* (Academic Press INC., New York, 1975).

[30] D. H. Froula, L. Divol, D. G. Braun, B. I. Cohen, G. Gregori, A. Mackinnon, E. A. Williams, S. H. Glenzer, H. A. Baldis, D. S. Montgomery, *et al.*, Phys. Plasmas **10**, 1846 (2003).

[31] D. E. Evans, Plasma Physics **12**, 573 (1970).

[32] D. H. Froula, L. Divol, H. A. Baldis, R. L. Berger, D. G. Braun, B. I. Cohen, R. P. Johnson, D. S. Montgomery, E. A. Williams, and S. H. Glenzer, Phys. Plasmas **9**, 4709 (2002).

[33] S. H. Glenzer, C. A. Back, K. G. Estabrook, R. Wallace, K. Baker, B. J. Macgowan, B. A. Hammel, R. E. Cid, and J. S. De Groot, Phys. Rev. Lett. **77**, 1496 (1996).

[34] D. H. Froula, L. Divol, N. B. Meezan, S. Dixit, J. D. Moody, P. Neumayer, B. B. Pollock, J. S. Ross, and S. H. Glenzer, Phys. Rev. Lett. In Press (2007).

[35] C. Tang, J. Appl. Phys. **37**, 2945 (1966).

[36] D. S. Montgomery and R. P. Johnson, Rev. Sci. Instrum. **71**, 979 (2001).

[37] N. B. Meezan, R. L. Berger, L. Divol, D. H. Froula, D. E. Hinkel, O. S. Jones, R. A. London, J. D. Moody, M. M. Marinak, C. Niemann, et al., Phys. Plasmas Submitted for Invited APS-DPP (2007).

[38] T. Dewandre, J. Albritton, and E. Williams, Phys. Fluids **24**, 528 (1981).

[39] P. Kaw, G. Schmidt, and T. Wilcox, Phys. Fluids **16**, 1522 (1973).

[40] E. A. Williams, Phys. Plasmas **13**, 056310 (2006).